Design, fabrication and physical analysis of TiN/AlN deep UV photodiodes

Hassan Ali Barkad, Ali Soltani, Maghnia Mattalah, J-C Gerbedoen, Michel Rousseau, Jean-Claude de Jaeger, Ali Benmoussa, Vincent Mortet, Ken Haenen, Brahim Benbakhti, et al.

Design, fabrication and physical analysis of TiN/AlN deep UV photodiodes

H. A. Barkad[1], A. Soltani[1]*, M. Mattalah[1], J-C. Gerbedoen[1], M. Rousseau[1], J-C. De Jaeger[1]
[1] IEMN, UMR-CNRS 8520, Avenue Poincaré, Université de Lille1, 59652 Villeneuve d'Ascq, France

A. BenMoussa[2]
[2] Royal Observatory of Belgium (ROB, STCE), Circular Avenue 3, B-1180 Brussels, Belgium

V. Mortet[3], K. Haenen[3]
[3] Institute for Materials Research, Hasselt University, Wetenschapark 1, B-3590 Diepenbeek, Belgium
IMEC vzw, Division IMOMEC, Wetenschapark 1, B-3590 Diepenbeek, Belgium

B. Benbakhti[4]
[4] DEEE, Rankine Building, Oakfield Avenue. University of Glasgow, G12 8LT Glasgow, Scotland, UK

M. Moreau[5]
[5] LASIR, USTL, C5, BP 69, 59652 Villeneuve d'Ascq Cedex, France

R. Dupuis[6]
[6] CCS-SECE, Georgia Institute of Technology, 777 Atlantic Drive NW, Atlanta, GA 30332-0250, USA

A. Ougazzaden[7]
[7] Georgia Tech-Lorraine (GTL), UMI 2958 GT-CNRS, 2-3 rue Marconi, 57070 Metz, France

Abstract

Deep-ultraviolet solar-blind photodiodes based on high-quality AlN films grown on sapphire substrates with a metal-semiconductor-metal configuration were simulated and fabricated. The Schottky contact is based on TiN metallisation. The material is characterised by micro-Raman spectroscopy and X-ray diffraction technique. The detector presents extremely low dark current of 100fA at -100V DC bias for a device area of 3.1 mm^2. It also exhibits a rejection ratio between 180nm and 300nm of three orders of magnitude with a very sharp cut-off wavelength at 203nm (~6.1eV). The simulation, based on a 2D energy-balance model using COMSOL® software, permits to help the designer for the optimum topology determination by means of physical studies. The measurement results are in good agreement with the model predictions.

Keywords: Photodiodes, AlN, deep UV, Simulation.

* *Corresponding author*: ali.soltani@iemn.univ-lille1.fr

Introduction

Solar-blind deep-ultraviolet (DUV) photodetectors are able to operate at high temperature and in harsh environment thanks to their wide band gap structure. These devices present a variety of potential applications in the fields of automotive, aerospace, and military industries, as well as in environmental and biological research. These applications require high-performance solar-blind photodetectors with low dark current and high UV responsivity. DUV photodetectors fabricated from various wide band gap semiconductors such as wurtzite aluminium nitride (wAlN) [1], cubic boron nitride (cBN) [4] and diamond [5], were reported recently.

AlN is the only semiconductor with a large direct band gap (~6.1eV) and it is available due to recent advances in epitaxial growth techniques [6] with very high quality epilayers obtained by metal-organic vapour physical epitaxy (MOVPE). In this paper, the design of the photodiodes is optimized by means of a 2D energy balance simulation based on COMSOL® software.

The fabricated devices have a Metal/Semiconductor/Metal (MSM) configuration with circular inter-digitated electrodes. The device's spectral response reveals a very sharp cut-off wavelength at 203nm (~6.1eV).

Material characterization

AlN films are deposited on sapphire (Al_2O_3) substrate by MOVPE. The growth temperature is 1100°C under 100Torr growth pressure. Trimethylaluminum and ammonia are used as the source materials and the carrier gas is hydrogen [6]. The AlN wurtzite structure belongs to the space group $C^4_{6\upsilon}$ $P6_3/mmc$, associated to the irreducible representation $\Gamma=A_1+2B_1+E_1+2E_2$ [7]. Crystalline phases and growth directions of AlN films were determined by $\theta/2\theta$ X-Ray Diffraction (XRD) with CuKα (k=1.540598Å) radiation operated at 40kV and 30mA. The rocking curve scan was performed with a detector at 2θ=36.1° corresponding to the 2H-AlN (0002) reflection (JCPDS c25-1133) when the sample orientation θ was varied from 5° to 30°.

The FWHM of the (0002) peak measured in the θ-2θ XRD pattern of AlN film is 0.77° and its associated rocking curve 0.3°. The thickness of the thin film is 820nm.

The material quality is crucial since the optical performance in the extreme UV (EUV) is strongly influenced by the surface characteristics. High quality active layer is required and the thickness for total absorption should be optimal to obtain less defects, crack-free layers, low roughness, and good structural homogeneity. The doping level of the active layer is also one of the most critical parameters and should be below $10^{15}cm^{-3}$ in order to achieve a depletion reach-through region for a reasonable electrode gap spacing and very low dark current.

Micro-Raman spectra are obtained using a Jobin Yvon spectrometer with three excitation sources at λ=266nm, 514nm and 785nm (see Figure 1). Optical modes marked by a star and a square correspond to sapphire substrate and the AlN thin film respectively. All the TO and LO modes of AlN and sapphire can be seen on the spectra of Danidov *et al.* [7] and McNeil *et al.* [8] demonstrating the crystalline state of the deposited AlN films. Table 1 gives a comparison of our results with those of references [7] and [8]. The spectrum under UV (@ 266nm) excitation exhibits clearly the A_1(TO) at $621cm^{-1}$, the E_2^2(T0) at $660cm^{-1}$ and the A_1(LO) at $891cm^{-1}$. The E_1^2 mode at $247cm^{-1}$ is only observable under visible (λ=514nm) or near infrared (λ=785nm). These values are close to those of AlN crystal [7, 8].

Modelling

In order to design and fabricate AlN based photodetectors for solar-blind applications, a 2D energy-balance model using COMSOL® software was developed. This model is based on the conservation equations deduced from Boltzmann's equation and coupled to Poisson's equation as such:

$$\text{div}(-\varepsilon\, \text{grad}V)=q(n-p+N_A^+-N_D^-)$$

where ε is the permittivity, n the electron density, q is the absolute electron charge, N_A^+ et N_D^+ correspond ionized acceptors and donors density respectively.

Charge conservation equations:

For electrons: $\frac{\partial n}{\partial t} + div(n\vec{v_n}) = G - U \quad with \quad v_n = -\mu_n \left[n\vec{E} + \left(\frac{1}{n}\right) div\left(nk_B T_e\right) \right]$,

For holes: $\frac{\partial p}{\partial t} + div(n\vec{v_p}) = G - U \quad with \quad v_p = \mu_p \left[p\vec{E} - \left(\frac{1}{p}\right) div\left(pk_B T_e\right) \right]$

Where G corresponds to electron-hole generation which is defined as: $G(x)=\phi(1-\Re)\alpha\, e^{-\alpha x}$ with $\Re(\lambda)$ the reflection coefficient and $\alpha(\lambda)$, the absorption coefficient versus wavelength. μ is the carriers mobility.

U is the bulk recombination rate, defined as: $U=U_{rad}+U_{SRH}+U_{Aug}$, where U_{SRH} corresponds to Shockley-Read-Hall rate recombination, U_{rad} is the radiative recombination rate and U_{Aug} is the Auger recombination rate.

The equations governing the energy flux are for electrons:

$\frac{\partial(nw)}{\partial t} = -div\left[\left(w + k_B T_e\right).n\vec{v}_n \right] - n\vec{v}_n \vec{E} - \frac{n\left(w - w_0\right)}{\tau_w(w)}$, where τ_w is the energy relaxation time and w is the average energy related to the average velocity $\vec{v}_n$ and electron temperature T_e.

$w = \frac{1}{2} m^* v_n^2 + \frac{3}{2} k_B T_e$, $w_0 = \frac{3}{2} k_B T_L$, where k_B is the Boltzmann's constant.

The transport parameters such as electron mobility, energy relaxation time and electron effective mass, are obtained from stationary Monte-Carlo simulations at room temperature. In the charge conservation equation, a generation term is included to take into account the light excitation. In this model, the number of electron-hole pairs created per absorbed photon is always unity in the wavelength region 170-425 nm (no secondary ionizations).

Furthermore, the band-to-band and Shockley-Read-Hall recombination effects are introduced. From this model, numerical simulations are carried out to study and optimize the device parameters such as detector geometry (gap spacing and electrodes width) and applied bias.

The studied structure is a MSM photodiode. The 2D simulation is carried out for a 300 nm thick AlN (unintentionally doped n-type at $10^{15} cm^{-3}$). The Schottky barrier height is 1eV and the total area is

(10×10) μm^2 corresponding to a screen pixel whatever the considered topology. The photocurrent is calculated at 10V bias (V_{AK}) and the excitation power is fixed to 12 $\mu W/cm^2$ from 170 nm to 425 nm according to the available data of the absorption coefficient and the reflectivity of AlN [10].The photodiode design was optimized considering the different main parameters. The first structure parameter to be optimized is the finger spacing for a given bias. Figure 2 shows the evolution of the device responsivity versus the electrode spacing for a symmetric design with two fingers. In the simulation, the electrode length is 0.2 µm and the electrode spacing varies from 0.5 µm (submicron structure) to 8 µm. The V_{AK} bias between the two electrodes varies from 0.1 V up to 15 V. The responsivity increases with this bias as it was expected and it is important to notice that it becomes higher for submicron devices [11].

The second structure parameter to be optimized is the finger width and device symmetry. For this study, different finger widths and device symmetries were simulated at 10V. Figure 3 shows the theoretical evolution of the responsivity versus the photon energy for different symmetric (sym) or asymmetric (asym) topologies as anode width A_L, cathode width K_L, number of fingers N, spacing between electrodes S and the fill factor *K* (active area/AlN area ratio). It can be noted that the responsivity increases when the finger width becomes submicron. The shadowing of the active area by the interdigitated contacts is the main drawback of the MSM-detector and results in loss of efficiency; furthermore the photoresponsivity is driven by the device fill factor becoming worst for the asym1 structure.

The dark current was also simulated for different spacing S showing a difference of several magnitudes for submicronic devices. Furthermore, an increase of this current versus V_{AK} is observed for a lower value of V_{AK} when the spacing drops. Consequently, a compromise must be found between the dark current level and the photoresponse.

To improve the device responsivity, semitransparent electrodes associated to a submicronic spaced and asymmetric topology can be considered on a large area device. All these solutions provide better

detector characteristics in terms of dark current, UV/visible contrast, linearity and enhancement in responsivity.

Device fabrication

The devices were fabricated by depositing TiN/Au Schottky contacts [12] on the AlN surface using magnetron sputtering deposition. First, the AlN films are cleaned with an aceton/isopropanol standard process and then etched in Ar^+ plasma with a substrate bias of -170 V for 90 s just before metal deposition in order to remove the native oxide on the AlN surface. Then, Au/TiN (150/5 nm) metallization is deposited on the AlN surface. An optical lithography is used to define the patterns. The electrodes are obtained after an Au etching with a potassium iodide solution (KI) and a TiN etching using H_2SO_4/H_2O_2 (piranha) solution. After deposition, the samples are annealed at 500°C for 40 min in N_2 atmosphere to improve the stability of the electrode contacts and to form the Schottky contact. To achieve high homogeneity of the electric field between the contacts, the electrodes are patterned with a circular interdigitated configuration (see Figure 4). The diameter of the devices varies from 1 to 3 mm diameter. The finger width is 2 µm, and the interspacing between the contact pads is 5 µm. The electrode fill factor is more than 62%. The advantage of this structure is a better noise factor in dark condition compared to submicronic devices [13].

Results and discussion

Current-voltage (I-V) characteristics are obtained using an Agilent 4155C with femtoampere (fA) resolution. Figure 5 shows the typical I-V characteristics of AlN-based MSM detectors measured in dark at room temperature in N_2 atmosphere before and after annealing. The device exhibits a very low dark current around 100 fA at ±100 V bias after annealing. The differential resistance measured between two fingers at a distance of 8 µm, varies from 2.1×10^{14} Ω to 1.5×10^{15} Ω before and after annealing, respectively between 0V and ±100V bias. The fabricated device exhibits a breakdown voltage (V_{BR}) higher than 100V corresponding to an electric field of 125 kV/cm.

Figure 6a shows the responsivity spectral measurement carried out on 2 mm diameter devices at ±100V DC bias, in the wavelength range from 180 nm to 300 nm (6.85 eV to 4 eV). The AlN MSM photodiodes have a peak responsivity around 2×10^{-3} A/W at 200 nm and a very sharp cut-off around 203 nm (6.1eV). This cut-off wavelength is close to AlN based MSM photodetectors obtained by Dahal et *al*. [14]. A rejection ratio of more than three orders of magnitude is observed between 200 nm and 300 nm. With our responsivity of 2 mA/W, the experimental specific detectivity @ 200 nm ($V_{AK}=\pm$ 100V) correspond to 1.054×10^{14} $cm^2H^{1/2}/W$.

Note that different solar-blind UV photodetectors based on wide band gap semiconductors have been reported. MSM diamond photoconductor [5] presented a rejection ratio of 1.6×10^4 between 210 nm (maximum photoresponse of 48 mA/W) and 400 nm at 5 V bias (S=5 and W=2 µm). MSM photodiode fabricated on cBN [4] films grown on silicon substrate showed at -30V a rejection ratio of four order of magnitude between the maximal response (i.e. 180 nm, 21 mA/W) and 250 nm (S=5 and W=2 µm). Finally AlN MSM photodiode [3] presented a rejection ratio of 1.2×10^4 between 200 nm (maximum photoresponse of 4.5 mA/W) and 360 nm at 30 V bias (S=4 and W=2 µm).

Spectra of the sub-band gap absorption are usually decomposed into “band to defect” and “band to tail” type transitions. In the first case, the photocurrent I_{ph} proportionally varies to the capture cross section of traps by the relationship: $\sigma(h\nu)\equiv\Delta I_{ph}/(I_{dark}.\phi_0.t)$ (1) with $\Delta I_{ph}=I_{ph}- I_{dark}$. The illumination time is 62 ms and the incident photon flux per cm^2 is $\phi_0=P/(S.E)$ where P is the incident power and E the photon energy. The active area is equal to 2.2 mm^2. The results of the fitting parameters obtained from Inkson’s model [15] are listed in Table 2. Three trap levels are deduced at 3.5, 5.45 and 5.8 eV up to the valence band. The capture cross sections of ET_2 and ET_3 show that those transitions are indirect. The transition ET_3 is responsible for the exponential increase at the absorption edge commonly described by the Urbach’s rule [16] and follows the relation: $I_{ph}(E)=I_{ph0}\exp[(E-E_G)/E_U]$ (2), where I_{ph0} is a material parameter, E_G is the band gap and E_U is the Urbach energy representing the width of the exponential absorption edge. In the particular case of III-nitrides, the Urbach’s tale is mainly a consequence of the carrier interaction with lattice and lattice imperfections (defects,

impurities…). The photocurrent curve is fitted with the Urbach expression (2) with the different parameters E_G, I_{ph0} and E_U corresponding to 6eV, $4{,}45\times10^{-4}$ and 0.13 eV, respectively. Figure 6b corresponds to the simulated responsitivity using the optical constants of single crystal of AlN with two light polarization states: E⊥c and E//c (c is the optical axis). Data for simulation are taken from Adachi [10].The responsivity curve is fitted from (2) with different parameters E_G, I_{ph0} and E_U corresponding to 6.1 eV, 5.22 mA/W and 0.22 eV, respectively for E⊥c and 5.95 eV, 2.5 mA/W and 0.47 eV for E//c. The experimental values are close to the theoretical predictions considering bulk AlN material showing a good crystallographic quality of the deposited thin films.

Conclusion

In summary, solar-blind DUV MSM photodetectors were simulated and fabricated on high quality wurtzite AlN films by MOVPE with a circular inter-digitated electrode design. The device topology is optimized from a 2D energy-balance simulation where the generation and recombination terms are included. The Schottky contact is based on a TiN metallisation process. A very low dark current around 100 fA at ±100V DC bias is obtained. The photodetectors show a high sensitivity to DUV light and a sharp cut-off wavelength around 203nm, close to the band gap of bulk AlN. This corresponds to the shortest value reported up to now on this semiconductor. The rejection ratio (the ratio of responsivity between 200 nm and 300 nm) is found to be over three orders of magnitude.

References

[1] R. Dahal, J. Li, Z. Y. Fan, M. L. Nakarmi, T. M. Al Tahtamouni, J. Y. Lin, H. X. Jiang., Phys. Stat. Sol. (c) **5** (6) (2008) 2148-2151.

[2] J. Li, Z.Y. Fan, R. Dahal, M.L. Nakarmi, J.Y. Lin and H.X. Jiang, Appl. Phys. Lett. **89** (2006) 213510.

[3] A. BenMoussa, J. F. Hochedez, R. Dahal, J. Li, J. Y. Lin, H. X. Jiang, A. Soltani, J.-C. De Jaeger, U. Kroth, M. Richter, APL **92** (2008) 22108.

[4] A. Soltani, H.A. Barkad, M. Mattalah, B. Benbakhti, J.-C. De Jaeger, Y. M. Chong, Y. S. Zou, W. J. Zhang, S.T. Lee, A. BenMoussa, B. Giordanengo, J.-F. Hochedez, APL **92** (2008) 053501.

[5] A. BenMoussa, A. Soltani, K. Haenen, U. Kroth, V. Mortet, H. A. Barkad, D. Bolsee, C. Hermans, M. Richter, J.-C De Jaeger, J.-F. Hochedez, Semiconductor Science and Technology **23** (2008) 035026.

[6] H. J. Kim, S. Choi, D. Yoo, J.-H. Ryou, R. D. Dupuis, R. F. Dalmau, P. Lu, Z. Sitar, APL **93** (2008) 022103.

[7] V. Yu. Davydov, Yu. E. Kitaev, I. N. Goncharuk, A. N. Smirnov, J. Graul, O. Semchinova, D. Uffmann, M. B. Smirnov, A. P. Mirgorodsky, R. A. Evarestov, Phys. Rev. B **58** (19) (1998) 12899-12907.

[8] L. E. McNeil, M. Grimsditch, R. H. French, J. Am. Ceram. Soc **76** (1993) 1132-1136.

[9] M. Kadleikova, J. Breza, M. Vesely, Microelectronics Journal **32** (12) (2001) 955-958.

[10] S. Adachi, "Optical Constants of Crystalline and Amorphous Semiconductors: Numerical Data and Graphical Information", Kluwer Academic, Boston 149 (1999).

[11] T. Palacios, E. Monroy, F. Calle, F. Omnès, APL **81** (10) (2002) 1902.

[12] J-C. Gerbedoen, A. Soltani, M. Mattalah, J-C. De Jaeger, H. Lahreche, A. Telia, submitted to APL.

[13] A. Navarro, C. Rivera J. Pereira, E. Muñoz, B. Imer, S. P. DenBaars and J. S. Speck, APL **94** (2009) 213512.

[14] R. Dahal, T. M. Al Tahtamouni, Z. Y. Fan, J. Y. Lin, and H. X. Jiang, APL. **90** (2007) 263505.

[15] J.C. Inkson, J. Phys. C, Solid State Phys. **14** (1981) 1093.

[16] F. Urbach Phys. Rev., **92** (1953) 1324.

Figure captions

Table 1: Peak positions of Raman modes (in cm^{-1}) of different wurtzite AlN and Al_2O_3 structures [7]. Our sample corresponds to the AlN/Al_2O_3 structure.

Table 2: Results of the fitting parameters obtained from the fitting curve of Figure 7a. The different level of traps ET_1, ET_2, ET_3 and the parameters P_1 permit to determine the capture cross sections (σ).

Figure 1: Micro-Raman spectra collected from the AlN film grown on a sapphire substrate. The squares are assigned to wurtzite AlN modes and the stars are assigned to sapphire substrate modes.

Figure 2: Responsivity evolution versus the electrode spacing for a symmetric structure with two 0.2 µm length electrodes for different biases under radiation excitation (λ=6.1 eV).

Figure 3: Responsivity versus the photon energy for different topologies: A_L is the anode length, K_L is the cathode length, N is the electrode number and K is the corresponding fill factor. The distance S between 2 electrodes varies between 0.5 µm and 1 µm. V_{AK}=10V.

Figure 4: Optical microscopy image of a 2mm diameter AlN photodiode (a) and zoom view of the circular inter-digitated electrodes in the centre area (b).

Figure 5: Current-Voltage characteristics of a 2 mm diameter AlN photodiode measured in dark conditions at room temperature before and after annealing at 500°C.

Figure 6: Spectral responsivity of an AlN MSM photodiode measured at ±100V DC bias under irradiation in the 180-300 nm range (a). Simulated responsivity from data [10] for two light polarization states (E//c and E⊥c) (b).

Optical modes (cm^{-1})	AlN bulk single crystal [7]	wAlN thin film [7]	AlN (our sample)	Al_2O_3 Bulk [9]	Al_2O_3 (our sample)
E_2(low) E_2^1	252	248	247	419	420
A_1(TO)	614	610	621	431	435
E_1(TO)	660	670	-	445	452
E_2 (high) E_2^2	673	657	660	492	-
A_1(LO)	893	890	891	600	580
E_1(LO)	916	912	-	748	752

Table 1

capture cross sections		**E_T (eV)**	**P_1**	**$\sigma(cm^2)$**
$\sigma_C=P_1(h\nu- E_{T1})^{3/2}/h\nu$	ET_1	3.5	2.2×10^{-5}	-
$\sigma_C=P_1(h\nu-E_{T2})^{3/2}/h\nu$	ET_2	5.45	6×10^{-4}	1.25×10^{-11}
$\sigma_C=P_1(h\nu-E_{T3})^{3/2}/h\nu$	ET_3	5.8	0.018	1.426×10^{-11}

Table 2

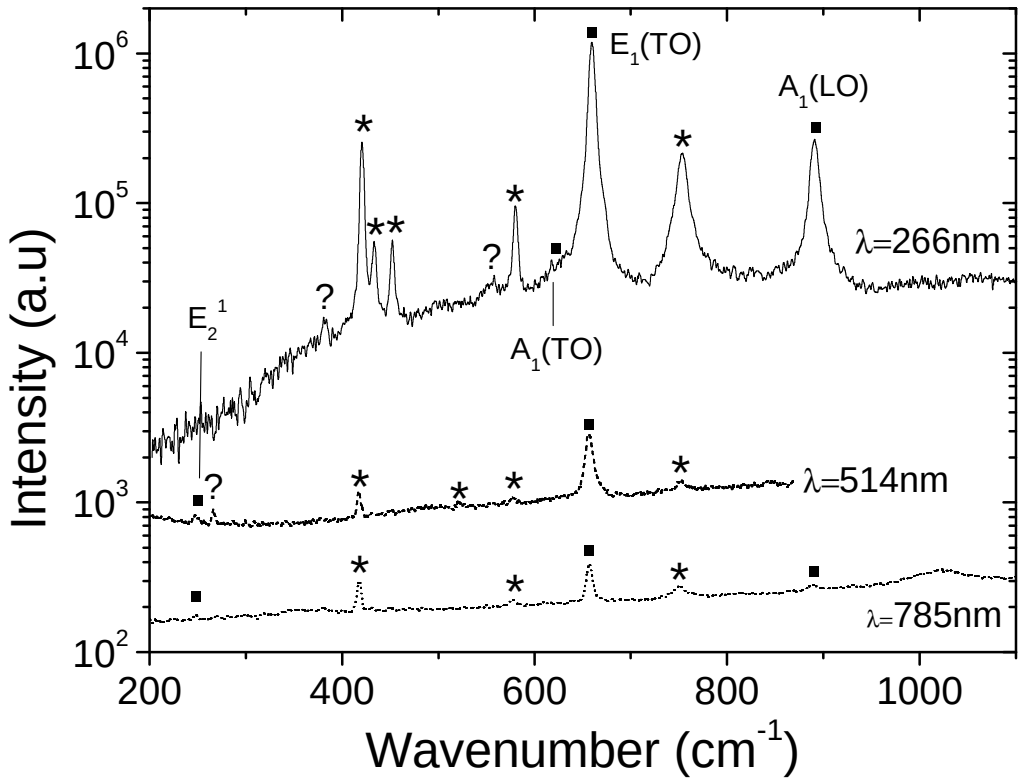
Intensity (a.u)
Wavenumber (cm-1)
E1(TO)
A1(LO)
A1(TO)
E2 1
λ=266nm
λ=514nm
λ=785nm

Figure 1

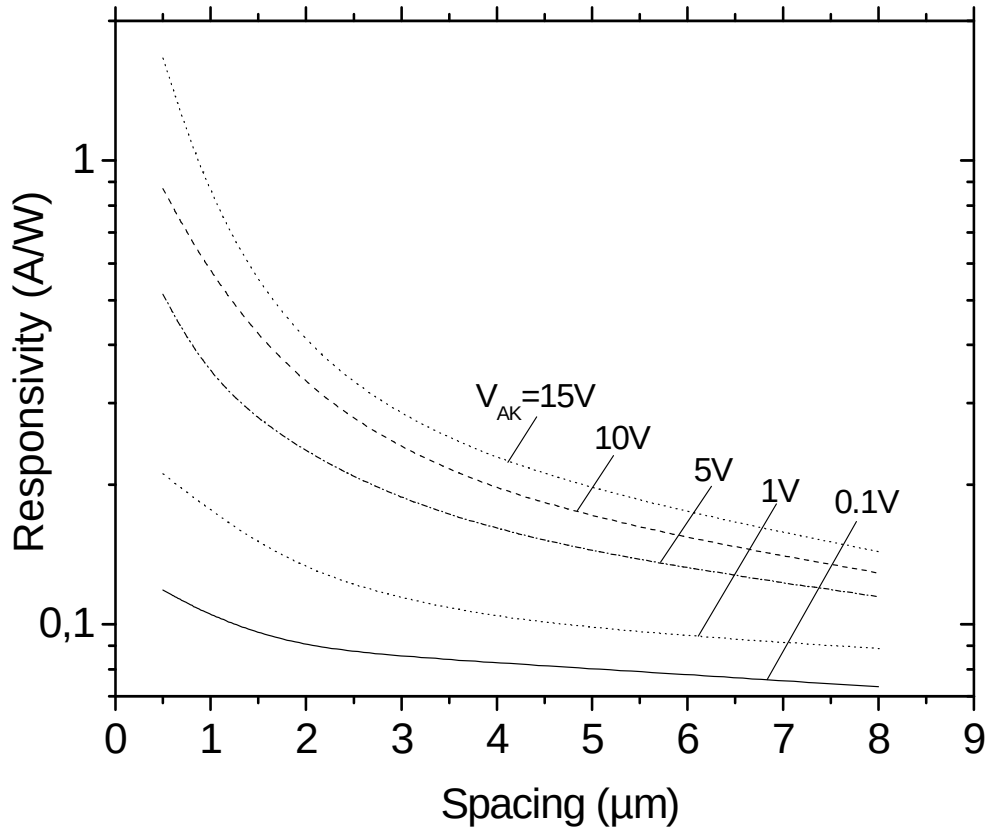
Responsivity (A/W)
1
0,1
0
1
2
3
4
5
6
7
8
9
Spacing (µm)
V_AK=15V
10V
5V
1V
0.1V

Figure 2

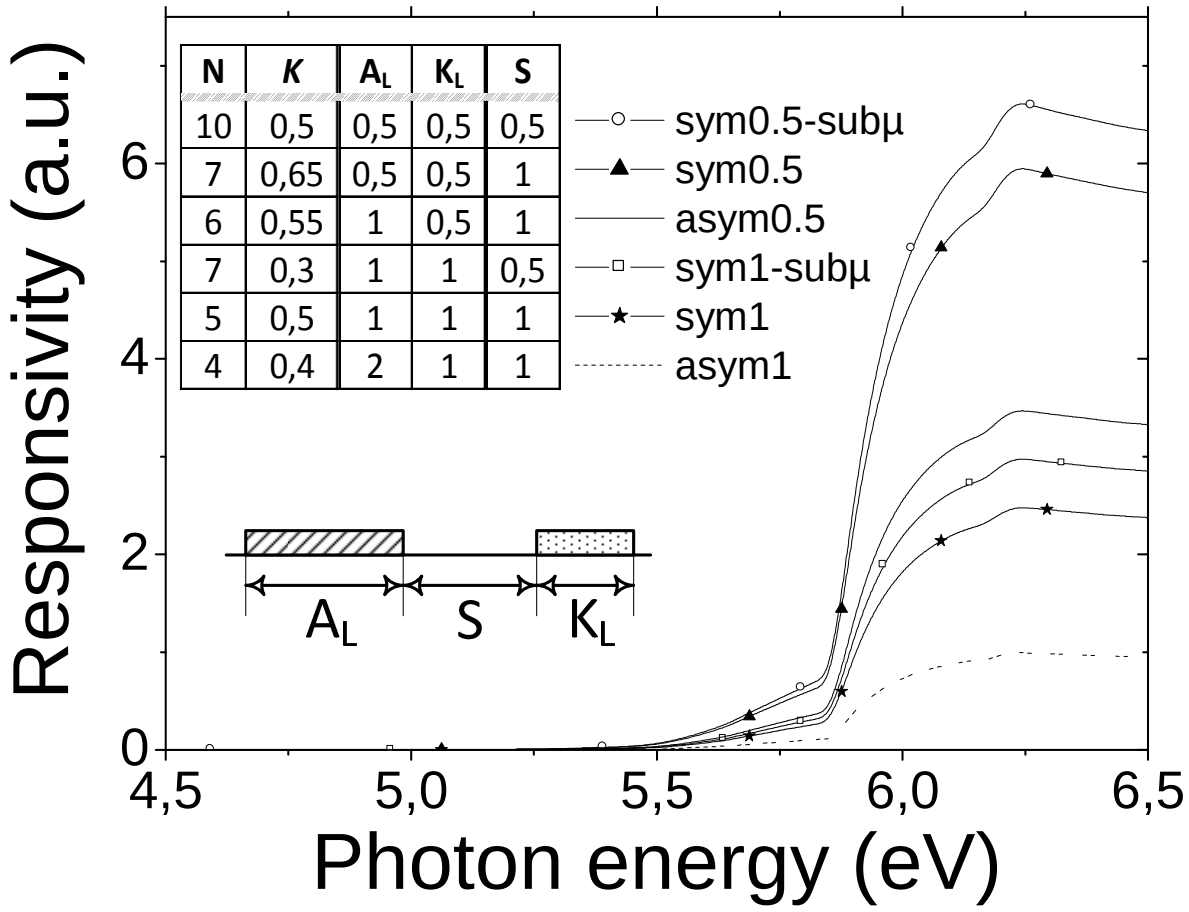
N
K
A_L
K_L
S
10 0,5 0,5 0,5 0,5
7 0,65 0,5 0,5 1
6 0,55 1 0,5 1
7 0,3 1 1 0,5
5 0,5 1 1 1
4 0,4 2 1 1
sym0.5-subμ
sym0.5
asym0.5
sym1-subμ
sym1
asym1
A_L
S
K_L
Responsivity (a.u.)
0
2
4
6
4,5
5,0
5,5
6,0
6,5
Photon energy (eV)

Figure 3

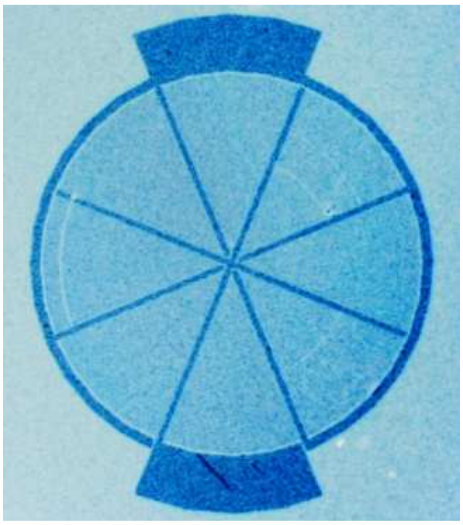

(a)

(b)

Figure 4

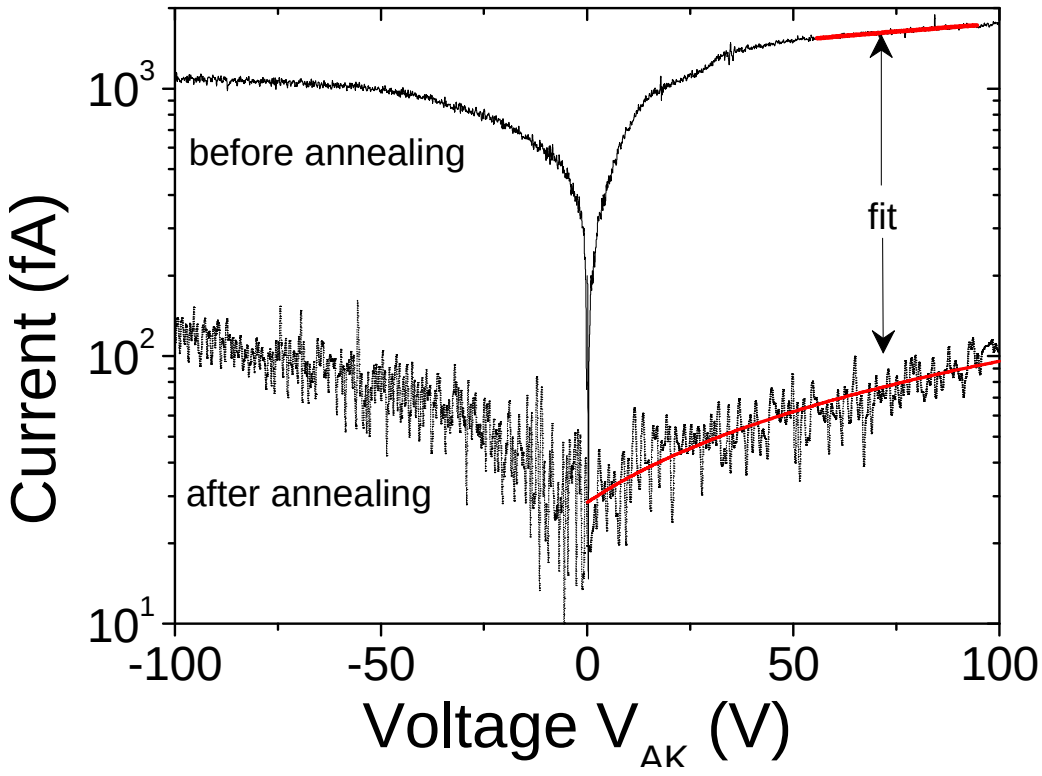
Current (fA)
10^3
10^2
10^1
before annealing
after annealing
fit
-100
-50
0
50
100
Voltage V_{AK} (V)

Figure 5

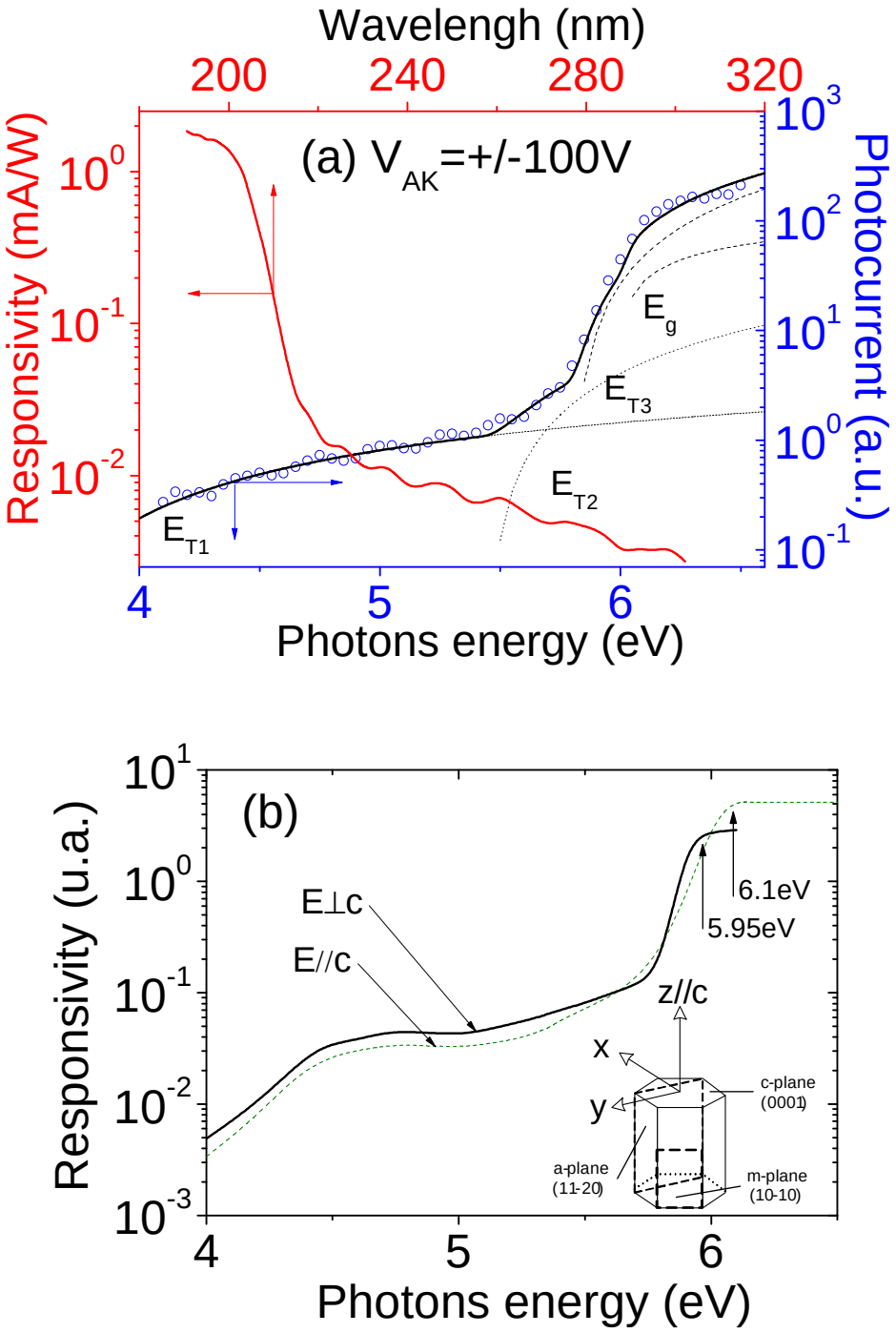
Wavelengh (nm)
200
240
280
320
(a) V_AK=+/-100V
Responsivity (mA/W)
Photocurrent (a.u.)
E_g
E_T3
E_T2
E_T1
Photons energy (eV)
(b)
Responsivity (u.a.)
E⊥c
E//c
6.1eV
5.95eV
z//c
x
y
c-plane
(0001)
a-plane
(11-20)
m-plane
(10-10)
Photons energy (eV)

Figure 6